**Activity patterns of metal oxide catalysts in the synthesis of N-phenylpropionamide from propanoic acid and aniline**

Francesco Arena; Chiara Deiana; Agata F. Lombardo; Pavlo Ivanchenko; Yuriy Sakhno; Giuseppe Trunfio; Gianmario Martra. Activity patterns of metal oxide catalysts in the synthesis of N-phenylpropionamide from propanoic acid and aniline. CATALYSIS SCIENCE & TECHNOLOGY. 5 pp: 1911-1918.
DOI: 10.1039/c4cy01504e

# Activity patterns of metal oxide catalysts in the synthesis of N-phenylpropionamide from propanoic acid and aniline†

Francesco Arena *a, Chiara Deiana b, Agata F. Lombardo a, Pavlo Ivanchenko b, Yuriy Sakhno a, Giuseppe Trunfio a and Gianmario Martra *b
aDipartimento di Ingegneria Elettronica, Chimica e Ingegneria Industriale, Università degli Studi di Messina, Viale F. Stagno D'Alcontres 31, 98166 Messina, Italy. E-mail: Francesco.Arena@unime.it; Fax: +39 090 391518; Tel: +39 090 393134
bDepartment of Chemistry and Centre for "Nanostructured Interfaces and Surfaces-NIS", University of Torino, via P. Giuria 7, 10125 Torino, Italy. E-mail: Gianmario.Martra@unito.it

---

The reactivities of various commercial and lab-made oxide samples (e.g., γ-Al2O3, CeO2, ZrO2 and TiO2) in the heterogeneous catalytic synthesis of N-phenylpropionamide (T, 383 K) from aniline and propanoic acid have been investigated. All the materials studied drive the direct synthesis of the amide to an extent depending on both the chemical and structural properties. A 0th-order kinetic dependence on the substrate concentrations suggests that the reaction proceeds via a Langmuir–Hinshelwood (L–H) pathway under kinetic control of the adsorption–desorption steps (the rate determining step, r.d.s.). The comparative analysis of the activity data on the basis of the relative surface specific kinetic constant discloses a superior surface reactivity of TiO2, CeO2 and ZrO2 over the γ-Al2O3 system, and also highlights marked differences in the catalytic functionality of the titania samples. IR spectroscopic studies of the carboxylic acids and amine adsorption and interaction patterns show the formation of the bidentate, bridging, and unidentate carboxylate intermediates accounting for the different amidation functionalities of the studied materials.

## 1. Introduction

The synthesis of amidic groups is a fundamental class of organic reactions for manufacturing a variety of biological compounds and innovative materials; in particular, besides widespread use in the agrochemical industry, ca. 65% of drug molecules include at least an amide unit,2 while amidic groups also represent the backbone of common polymeric materials.1,2

Although organic chemistry offers several methods for the lab-scale synthesis of amides, the main industrial manufacturing processes still rely on the reaction of amines with pre-activated carboxylic acid precursors, like anhydrides or acid chlorides.2,3 In turn, the latter are obtained from thionyl or oxalyl chloride or from carboxylic acids using stoichiometric amounts of coupling reagents (i.e., carbodiimides).2 All such methods suffer from severe environmental, safety, and economic drawbacks, including the use of noxious and/or dangerous reagents, and multiple reaction-purification steps resulting in a poor atom economy, while large amounts of harmful waste, requiring special disposal treatments, contribute to high E-factors.1,2 An alternative method involves the condensation of carboxylic acids with amines at high temperatures (>453 K), but is unfeasible for many functionalized substrates.2 On this account, the synthesis of amides has been recently indicated as a major green chemistry issue.2–17

Apart from the recognized effectiveness of microwave irradiation on the condensation of carboxylic acids with amines,4,6 and some catalytic redox routes using alternative reagents,5,8,9,16 the most attractive option for amide bond formation is the heterogeneous catalytic condensation of amines with carboxylic acids.10–15 Many solid acids such as boron–organic compounds,7 Fe3+/K10 montmorillonite,10 FeCl3, ZnCl2, zeolites, and silica-based catalysts,11 sulphated-tungstate,12 MCM-41,13 and Zr-salts,14 were shown to be active in the synthesis of amides using toluene under “azeotropic distillation” reflux conditions (383 K),1–14 while CeO2 showed the highest activity among many oxides in various transamidation reactions.15 In addition, Comerford et al. recently reported that silica and SBA materials are highly active in the synthesis of N-(phenyl)-phenylacetamide at 423 K in a continuous-flow reactor at short contact times,17 while mechanistic issues of the condensation of formic and acetic acid with 1-pentanamine on titania have been recently addressed.18 In this context, Grosjean et al. also emphasized the role of the reaction system, showing significant positive effects of heat input on the amidation kinetics because of faster rates of water removal.3

Therefore, this work is aimed at providing a comparative view of the reactivity patterns of various lab-made and commercial oxide catalysts (e.g., γ-Al2O3, TiO2, CeO2, ZrO2) in the condensation reaction of aniline with propanoic acid to N-phenylpropionamide using toluene as a solvent (T, 383 K). The kinetic analysis of the activity data reveals that the amidation functionality depends on both the chemical and structural properties of the materials studied, promoting the formation of different intermediates, as probed by IR spectroscopic measurements.

## 2 Experimental

### 2.1. Catalyst preparation

Commercial TiO2 (TiO2 P25 Evonik, ex Degussa, and TiO2 Merck) and γ-Al2O3 (000-1.5E Akzo Nobel) powders were used in their “as received” forms. The CeO2 sample was prepared by heating an aqueous solution of a Ce(NH4)2(NO3)6 precursor (Sigma Aldrich, >99%) under continuous stirring and refluxing at 373 K for 4 h. The resulting precipitate was filtered, washed, dried at 373 K for two days and finally calcined at 723 K for 3 h.19 The ZrO2 sample was prepared by dissolving a ZrOCl2·8H2O precursor (Sigma Aldrich, >99.5%) in distilled water, and adding a NaOH solution (0.25 M) at 298 K under vigorous stirring. After

digestion, the precipitate was filtered, washed until the chlorides completely disappeared, dried at 373 K overnight and further calcined in air at 873 K for 3 h. A list of the samples studied with their relative codes and specific surface area values is reported in Table 1.

Table 1 List of the studied catalysts

| Catalyst code | Supplier | SSA (m2 g−1) |
|---|---|---|
| γ-Al2O3 (000-1.5E) | Akzo Nobel | 261 |
| TiO2_Merck | Merck | 10 |
| TiO2_P25 | Evonik | 55 |
| CeO2 | Lab-made | 90 |
| ZrO2 | Lab-made | 21 |

2.2. Catalyst characterization

Specific surface area (SSA) values were determined from nitrogen adsorption isotherms (77 K) obtained using a ASAP 2010 (Micromeritics Instrument) gas adsorption device. Before measurements were conducted the samples were outgassed at 423 K until a residual pressure of ca. 0.2 mbar was achieved. The isotherms were elaborated by the BET method for the SSA calculations.

IR spectroscopy measurements were performed using a Bruker Vector 22 spectrometer equipped with a DTGS detector (4 cm−1 resolution); self-supporting pellets (ca. 10 mg cm−2) of the catalyst powders were placed into an IR cell with CaF2 windows and connected to vacuum lines (P < 10−5 mbar) to carry out in situ thermal treatments and adsorption–desorption tests.17 The samples were treated at 723 K under a dynamic vacuum for 1 h, then 6 mbar of O2 was admitted at the same temperature (for 1 h) to restore the original oxidation states of the oxides. Subsequently, the samples were cooled down to 473 K, still under O2 and then, to room temperature under vacuum. After the collection of the spectra of the treated catalysts in vacuum (background), high-purity vapors of propanoic or formic acid and then of 1-pentanamine (Sigma Aldrich) were added onto the catalysts for IR spectra collection. In the case of the sequential adsorption of propanoic acid and 1-pentanamine a set of measurements was further carried out after heating the pre-saturated samples at 383 K for 30 minutes. The spectra were reported in absorbance after subtraction of the background spectra, while the adsorbed species were analyzed by High Resolution Mass Spectrometry (HR-MS). After the spectroscopic measurements the pelletized samples were ground and suspended in 0.5 mL of Milli-Q water. Subsequently, the suspension was shaken in a Vortex mixer for 15 min and then centrifuged at 104 rpm for 5 min. The supernatant was then removed and the solid was treated a second time in 0.5 mL of Milli-Q water. Then, the two obtained solutions were mixed and analyzed in a LTQ Orbitrap mass spectrometer (Thermo Scientific) equipped with an atmospheric pressure interface and an electrospray ionization (ESI) source. The source voltage was set to 4.48 kV. The heated capillary temperature was maintained at 538 K. The tuning parameters adopted for the ESI source were: capillary voltage, 0.02 V; tube lens, 24.77 V; for the ion optics: multipole 0 offset, −4.28 V; lens 0 voltage, −4.36 V; multipole 0 offset, −4.28 V; lens 1 voltage, −13.69 V; gate lens voltage, −8.84 V; multipole 1 offset, −18.69 V; front lens voltage, −5.09 V. The mass accuracy of the recorded ions (vs. calculated) was ±1 mmu (without internal calibration). The samples, added to 100 μL of a 0.1 M HCOOH aqueous solution, were

delivered directly to the mass spectrometer via a Hamilton microliter syringe at a constant flow (10 µl min−1).

2.3. Catalyst testing

Catalytic tests were carried out in a magnetically stirred three-neck glass flask reactor, operating in batch mode and equipped with a thermometer, a reflux condenser, and a Dean-Stark device, for continuous water removal by “azeotropic distillation”.3 The reactor was loaded with 10 mL of toluene (solvent), 0.1 mL of n-octane (internal standard), 6 mmol (0.45 g) of propanoic acid and 0.2 g of the powdered catalyst (dp < 0.1 mm). The suspension was heated to 383 K, then a stoichiometric amount of aniline (6 mmol, 0.56 g) was slowly added. Evidence for the absence of internal mass-transfer resistances is given by the Weisz–Prater criterion

$$C_{W-P} = \eta \cdot \varphi_s^{\,2} = \frac{r_p^{\,2} \cdot (-r)}{D_{An/Tol} \cdot C_{An}} < 3 \times 10^{-3} \qquad (1)$$

(where rp and (−r) are the particle radius (cm) and the rate per unit of volume of catalyst (mol cmcat−3 h−1), while DAn/Tol (0.09 cm2 h−1) and CAn (0.55 mmol cm−3) are the diffusivity and concentration of aniline, respectively), as under the adopted conditions CW–P is always orders of magnitude smaller than one.20

Reaction mixture samples were withdrawn from the reactor and analyzed by a GC (7890A, Agilent Technologies) equipped with a capillary column (Restek, Rxi-1ms cross-bond), connected to a FID for the determination of the propanoic acid and aniline conversion (±3%). Furthermore, after 24 h of reaction time the reaction mixture was cooled and filtered by a sintered glass funnel, and the catalyst was washed with hot ethanol for the complete solubilization of the amide, the yield of which was determined by gravimetric analysis after ethanol evaporation.

3 Results and discussion

3.1. Catalytic activity

The results of the catalytic tests in the synthesis of the N-phenylpropionamide at 383 K are summarized in Table 2 in terms of aniline and propanoic acid conversion and amide yield values after 24 h of reaction time. A preliminary test in the absence of any catalyst confirms the lack of reactivity of the substrates, while all the oxide catalysts drive the condensation reaction with amide yields between 4 and 47%, in satisfactory agreement with the conversion degrees of both reagents (Table 2). In particular, the lowest and highest yields refer to the TiO2_Merck and TiO2_P25 samples respectively, while alumina (24%) and ceria (27%) show intermediate activities, which are significantly better than ZrO2 (9%).

Table 2 Conversion data of aniline and propanoic acid, and N-phenylpropionamide yields with the various catalysts at 383 K (CPA = CAn, 0.55 mol L−1; Ccat, 18 g L−1)

| Catalyst | Conversiona (%) aniline, p. acid | Amide yieldb (%) |
|---|---|---|
| a From GC analysis. b From gravimetric analysis. | | |
| No (blank test) | 0, 0 | 0 |

| Catalyst | Conversiona (%) aniline, p. acid | Amide yieldb (%) |
|---|---|---|
| γ-Al2O3_000-1.5E | 22, 25 | 24 |
| TiO2_Merck | 5, 4 | 4 |
| TiO2_P25 | 47, 49 | 47 |
| CeO2 | 28, 27 | 27 |
| ZrO2 | 8, 10 | 9 |

These data preliminarily indicate that chemical, structural and textural properties concur to shape the reactivity of the various oxide systems,21 although a proper assessment of their amidation functionality requires the knowledge of their kinetic parameters.

The kinetic dependence has been properly ascertained by a series of tests conducted at different (stoichiometric) reagent concentrations (0.28–1.10 mol L−1) and a constant TiO2_P25 catalyst load. The results in Fig. 1A show straight-line conversion trends up to an extent of ca. 80%, indicating a very small, if any, kinetic effect of substrate concentration on the reaction rate and, thus, a 0th-order kinetic dependence (Fig. 1B). Despite the lack of systematic kinetic data for the other catalysts, this peculiar rate law seems not to be specific to the TiO2_P25 system as no changes in the reaction rate were found using double concentrations of the substrates (1.1 mol L−1) and the CeO2 material (36 g L−1), while Comerford et al. indicated a constant N-(phenyl)-phenylacetamide yield (0.34–0.39 g gcat−1 h−1) using a K60 silica catalyst in a flow reactor (T, 423 K) at various contact times for conversion degrees between 9 and 46%.17 In particular, this yield value corresponds to a rate of ca. 1.50 × 10−3 mol gcat−1 h−1 which is comparable to the value of 5.4 × 10−4 mol gcat−1 h−1 herein found for TiO2_P25 at 383 K (Fig. 1B).

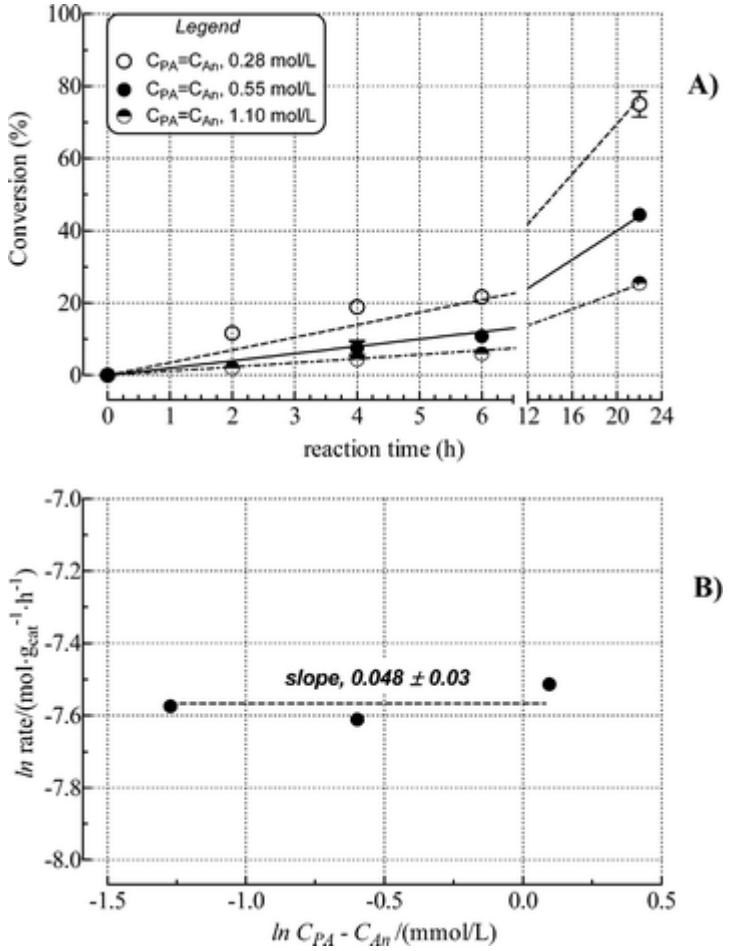


Fig. 1 (A) Average conversion of propanoic acid and aniline at 383 K at different stoichiometric concentrations on the TiO2_P25 catalyst (Ccat, 18 g L−1); (B) log-plot of rate data vs. reagent concentrations.

This evidence provides a convincing argument that the 0th-order kinetic dependence has a general validity irrespective of the catalytic material, likely as a consequence of the low operating temperature and characteristics of the “batch” reaction system (i.e., a high reagent-to-catalyst ratio).22

Besides, in the presence of (apolar) toluene as a solvent, an acid–base interaction of the reacting species drives the primary formation of an adduct,3,4

$$C_6H_5NH_2 + C_2H_5COOH \rightarrow C_6H_5NH_3^+\cdots{}^-OCOC_2H_5 \quad (2)$$

which undergoes a subsequent intramolecular rearrangement leading to the formation of the C–N bond and water elimination.

$$C_6H_5NH_2\cdots H\cdots OCOC_2H_5 \leftrightarrows C_6H_5{-}NH{-}CO{-}C_3H_5 + H_2O \quad (3)$$

The latter requires a proper activation step in order to trigger the nucleophilic attack of the C-atom by the N-atom of the amine species, this being the rate determining step (r.d.s.) of the amidation reaction.4 In this

context, the role of the solid catalyst consists of the adsorption–activation of the adduct on a Lewis acid center (α+) to restore the nucleophilic character of the nitrogen atom by a weakening of the "N⋯H" interaction,15,18,23 as shown in Scheme 1.

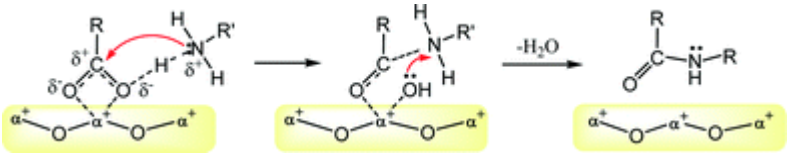


Scheme 1 Mechanism of the amidation reaction on the oxide catalysts.

Having ascertained the extensive adsorption of carboxylic acids, amines, and amides on the surface acidic sites of many oxide materials,15,18,23 it can be speculated that the heterogeneous catalytic amidation proceeds via a classic Langmuir–Hinshelwood (L–H) reaction pathway,22 although a dual-site mechanism, like that of amide transamidation,15 formaldehyde to methyl formate dismutation,24 and triacylglyceride to fatty methyl ester transesterification,25 cannot be ruled out in light of spectroscopic findings documenting the presence of acid–base pairs on ceria,15 titania,24,26 zirconia and alumina surfaces.24

In turn, the multi-step pathway of the catalytic reaction hinders a direct assessment of the r.d.s. because adsorption–desorption processes at the temperature of the catalytic tests (383 K) can affect the reaction kinetics.15,22,23 Then, at the first instance, product desorption is also considered to be a r.d.s.

$$R–COO–\ldots NH3+–R' + \alpha+ \leftrightarrows (RCOO–H3NR')ads \quad (4)$$

$$(RCOO–H3NR')ads \rightarrow (RCO–NHR')ads + H2O\uparrow \quad (5)$$

$$(RCO–NHR')ads \rightarrow RCO–NHR' + \alpha+ \quad (6)$$

In particular, the above simplified reaction mechanism predicts equilibrium conditions for the adsorption of the adduct on a Lewis acid site (4), while the amide formation (5) and desorption (6) steps are considered to be r.d.s. (e.g., rate = r5 = r6) and irreversible due to continuous water evaporation and slow amide desorption,23 respectively. The active site balance at steady-state conditions

$$[\alpha+]0 = [\alpha+] + [(RCOO–H3NR')ads] + [(RCO–HNR')ads] \quad (7)$$

leads to the following kinetic equation

$$\text{rate}\left(\text{mol } g_{cat}^{-1}\ h^{-1}\right) = \frac{k_5 \cdot K_4 \cdot [\text{RCOO–H}_3\text{NR}']}{1 + K_4 \cdot \left(1 + \frac{k_5}{k_6}\right) \cdot [\text{RCOO–H}_3\text{NR}']} \cdot [\alpha^+]_0 \quad (8)$$

where k5 (h−1) and k6 (h−1) are the kinetic constants of the relevant steps, K4 (L mol−1) is the equilibrium constant of the adduct adsorption and [α+]0 (mol g−1) is the catalyst density of the active sites. Eqn (8) proves that the experimental 0th-order kinetic dependence depends on large values of the adsorption constant K4 which means, in turn, an extensive coverage of the active sites by reagents, products, and/or intermediates.

On account of such evidence, the 0th-order constant (k0, mol L−1 h−1) has been calculated from the conversion data in Table 2, while, by dividing k0 by the catalyst concentration (kw, k0/Ccat) and the latter by the surface area values (kSSA, kw/SSA), the specific constants of the various catalysts per mass and SSA units were obtained, respectively (Table 3).

Table 3 0th-order (k0) and specific 0th-order constants (kw, kSSA) of the studied catalysts

| Catalyst | k 0 (mol L−1 h−1) | k W (mol gcat−1 h−1) | k SSA (mol mcat−2 h−1) |
|---|---|---|---|
| TiO2_P25 | 1.0 × 10−02 | 5.4 × 10−04 | 1.0 × 10−05 |
| ZrO2 | 2.1 × 10−03 | 1.2 × 10−04 | 5.5 × 10−06 |
| TiO2_Merck | 9.2 × 10−04 | 5.1 × 10−05 | 5.1 × 10−06 |
| CeO2 | 6.2 × 10−03 | 3.4 × 10−04 | 3.9 × 10−06 |
| γ-Al2O3 | 5.5 × 10−03 | 3.0 × 10−04 | 1.2 × 10−06 |

Constant values different by more than one order of magnitude (k0, 1.0 × 10−2–9.2 × 10−4 mol L−1 h−1) confirm the strong influence of the surface structure on the amidation functionality of the most (TiO2_P25) and least (TiO2_Merck) active titania samples.26 However, the influence of the surface area on kw (Fig. 2A) shows that the TiO2_P25 and γ-Al2O3 systems are significantly more and less active than expected from the linear relationship depicted by TiO2_Merck, ZrO2 and CeO2, respectively. Indeed, the kSSA values prove that γ-Al2O3 (1.2 × 10−6 mol mcat−2 h−1) and TiO2_P25 (1.0 × 10−5 mol mcat−2 h−1) have the worst and best functionalities respectively, while TiO2_Merck, ZrO2 and CeO2 are characterized by an intermediate reactivity, as proven by similar kSSA values, ca. five times larger than γ-Al2O3 (Fig. 2B).

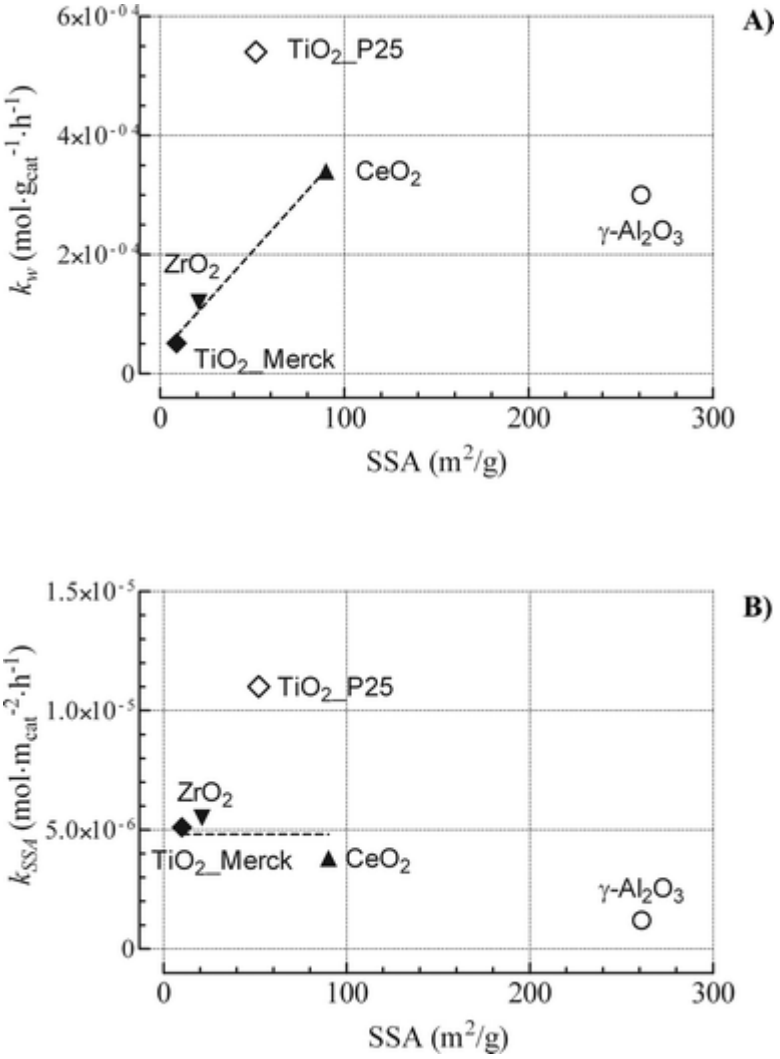


Fig. 2 Influence of the surface area on: (A) the specific 0th-order constant (kw), and (B) the specific surface constant (kSSA) of amide formation (T, 383 K) of the various catalysts.

The origin of the different reactivities of the studied oxides is addressed by IR measurements.

3.2. IR spectroscopy and mechanistic evidence

The amidation functionality of the various catalysts has been probed by a systematic IR study of propanoic acid adsorption and its reaction pattern toward 1-pentanamine (taken as a model amine for the sake of safety). The spectral data of the various oxides are shown in Fig. 3, while a summary of the various signals is reported in Table S1 in the ESI.† In all cases the adsorption of propanoic acid (blue lines) yields the formation of carboxylate species, according to the vasymCOO− and vsymCOO− modes in the 1650–1550 and 1450–1400 cm−1 ranges, respectively.27

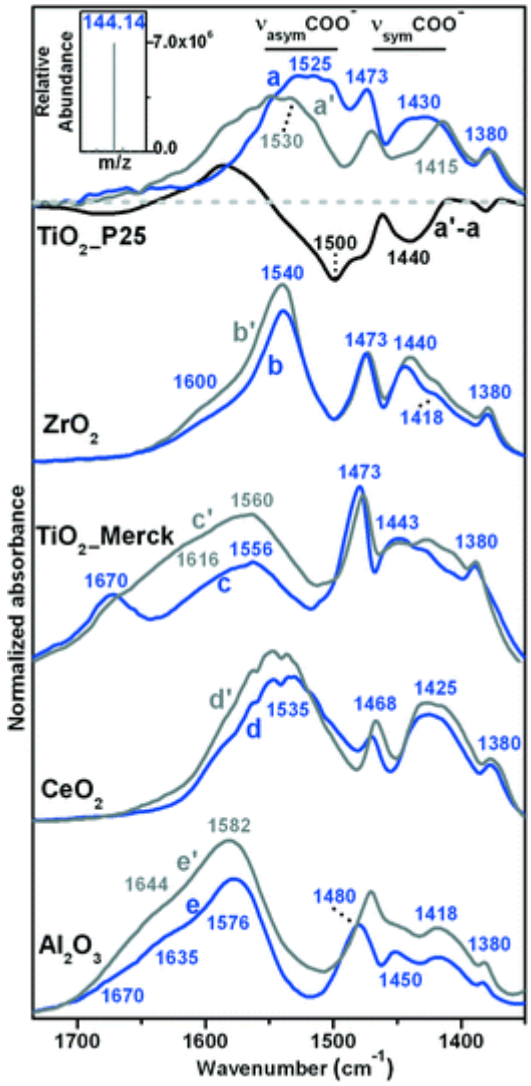


Fig. 3 IR spectra of TiO2_P25, ZrO2, TiO2_Merck, CeO2, and γ-Al2O3 in contact with propanoic acid and outgassed at r.t. (blue lines: a, b, c, d, e); and after the addition of 1-pentanamine (grey lines: a', b', c', d', e'.). The black curve of TiO2_P25 results from a'−a curve subtraction.

In the case of TiO2_Merck and γ-Al2O3 the νC═O component of the carboxylic group in C2H5COOH molecules in the non-dissociated form is also present (ca. 1670 cm−1). Moreover, the pattern in the case of CeO2 is visibly shifted to a lower frequency, probably reflecting the peculiar electronic properties of the lanthanides.28

The subsequent addition of 1-pentanamine on TiO2_P25 (Fig. 3a') causes a decrease in components due to propanoate species and the appearance of a tail in the 1650–1560 cm−1 range due to the νC═O mode of the amide species.29,30 The formation of the amide was confirmed by HR-MS data of the washing solution of the TiO2_P25 sample, showing a signal at m/z = 144.14 due to the protonated N-pentylpropanamide (Fig. 3, top-left inset). For all the other systems the adsorption of amine results in the superimposition of its IR pattern and no N-pentylpropanamide was detected in the washing solutions by HR-MS.

Furthermore, the IR signals of the adsorbed propanoic acid due to the carboxylate moieties appear to be composed of sub-bands, the position and relative intensity of which are characteristic for each oxide.

Although the broadness of the overall vasymCOO− patterns of TiO2_P25, TiO2_Merck and CeO2 hinders any reliable deconvolution of the various components, the difference between the spectra of TiO2_P25, after and before the amidation, indicates that the vasymCOO− and vsymCOO− components which vanish during the reaction are centered at 1500 and 1440 cm−1, respectively (Fig. 3, curve a'−a). These data provide a splitting value of only 60 cm−1, markedly lower than that of an ionic carboxylate like C2H5COONa (Table 4), suggesting, thus, the prevalent formation on this system of a bidentate carboxylate structure (Scheme 2).27

Table 4 Splitting between the vasymCOO− and vsymCOO− modes of propanoate species on the various catalysts and in the sodium salt for comparison

| Catalyst | ν asymCOO− | ν symCOO− | Δν |
|---|---|---|---|
| TiO2_P25 | 1500 | 1440 | 63 |
| ZrO2 | 1540 | 1440 | 100 |
| TiO2_Merck | 1556 | 1443 | 113 |
| CeO2 | 1535 | 1425 | 110 |
| γ-Al2O3 | 1576 | 1450 | 126 |
| C2H5COONa | 1560 | 1430 | 130 |

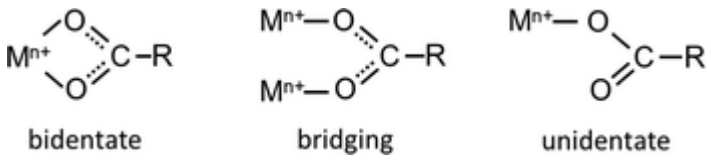


Scheme 2 Carboxylate structures stabilized on an oxide surface with Mn+ being the metal (e.g., Ti4+, Zr4+, Ce4+, Al3+) cation (ref. 27).

The lack of straight correlations in the evolution of sub-bands at high and low frequencies hinders the recognition of vasymCOO− and vsymCOO− pairs in the other cases. Besides, it can be considered that i) the angle between the two branches of –COO− oscillators is expected to be larger than 90°, and ii) in both the bridging and bidentate structures such oscillators can be reasonably assumed to be sufficiently equivalent in order to apply the well-known relationship

$$(I_{sym}/I_{asym}) = ctg^2(\theta/2) \quad (9)$$

where θ is the angle between the two branches.31 As a consequence, in each pair of signals the one due to the vasymCOO− mode should exhibit a higher intensity with respect to its vsymCOO− partner. On such a basis, the most intense components of the vsymCOO− patterns observed for the adsorption of propanoic acid on catalysts other than TiO2_P25 should be paired to the most intense vasymCOO− ones. The calculated Δν splitting values (Table 4) indicate that the prevailing fraction of carboxylate groups should be

of the bridging type (Scheme 2) on ZrO2, TiO2_Merck, CeO2 and γ-Al2O3. The formation of different amounts of carboxylate species on the titania samples is still to be related to the surface features of the TiO2_P25 and TiO2_Merck materials.26

Although different intermediates and activity evidence confirm the superior amidation functionality of the TiO2_P25 sample, these data do not provide information on differences among the other catalysts, as they are all inactive toward amidation under the “model” in situ conditions and at room temperature.

On this account, the catalysts subjected to the adsorption of propanoic acid and 1-pentanamine were heated to 383 K and further cooled down to r.t. for IR measurements (Fig. S1 of the ESI†). TiO2_P25 shows a further consumption of the components of the carboxylate moieties, while the weak band at 1630 cm−1 rises in intensity, due to the νC═O mode of the amide group.29,30 Negligible changes in the spectral pattern of γ-Al2O3 further prove its poor catalytic functionality, while a strong decrease of all the signals hinders any reliable assessment of the various species on the ZrO2, TiO2_Merck and CeO2 samples, likely as a consequence of significant desorption (and condensation on colder points of the IR cell) phenomena.

Then, a series of measurements was carried out using formic acid, since it is expected to be more reactive because of the lack of inductive effects of the alkyl substituent.18 The spectral features of formic acid adsorption (Fig. 4, blue lines) account for the formation of the carboxylate species on TiO2_P25, ZrO2 and CeO2 (typical vasymCOO− and vsymCOO− patterns in the 1600–1500 and 1400–1300 cm−1 ranges, respectively), and are shifted to a lower frequency for CeO2 (vide supra). The components of the HCOOH molecules in non-dissociated forms in the spectra of TiO2_Merck and γ-Al2O3 are also evident. A summary of the assignment of the signals on the various catalysts is reported in Table S2 of the ESI.†

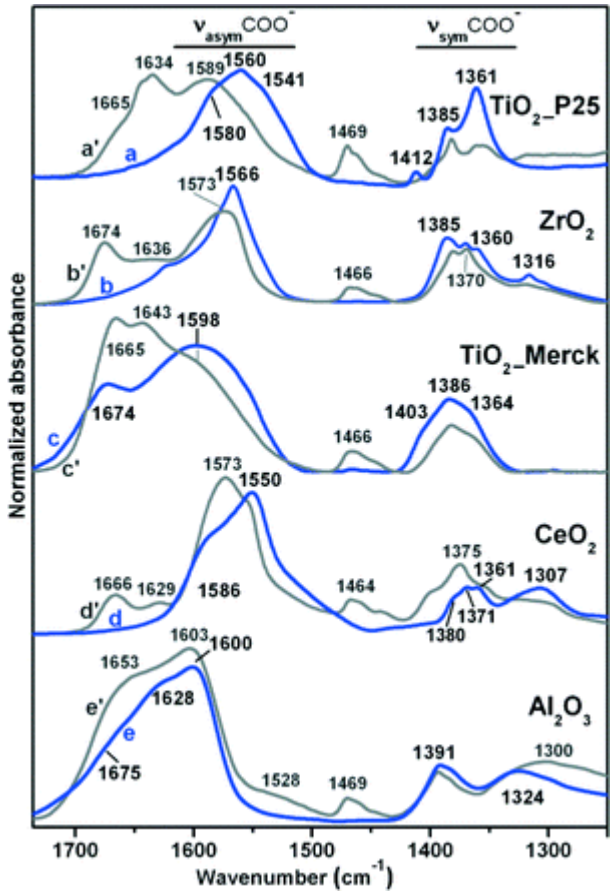

Fig. 4 IR spectra of TiO2_P25, ZrO2, TiO2_Merck, CeO2, and γ-Al2O3 in contact with formic acid and outgassed at r.t. (blue lines: a, b, c, d, e); and after the addition of 1-pentanamine (grey lines: a', b', c', d', e').

The addition of 1-pentanamine causes a decrease of the components due to formates and the appearance of signals in the range 1700–1600 cm−1, due to the νC═O mode of the amide species,29,30 except for the γ-Al2O3, in which the addition of the amine basically gives rise only to the appearance of the spectral patterns of newly adsorbed molecules. On the contrary, TiO2_P25 shows the strongest decrease of the vasymCOO− and vsymCOO− signals. Notably, on the whole these data are in a fairly good agreement with the activity scale (TiO2_P25 > ZrO2 ≈ TiO2_Merck ≈ CeO2 > γ-Al2O3) of amidation tests (Fig. 2).

As already observed in the case of propanoic acid, the spectral features of the formate species also result from the overlapping of sub-bands, despite the fact that in several cases they are better resolved. In addition, the absence of the signal due to the deformation modes of the –CH2 and –CH3 groups allows for a clearer recognition of the vasymCOO− and vsymCOO− patterns. Thus, a deconvolution analysis of the formate patterns has been performed, setting the position of the various components by the 2nd-derivative method (Fig. 5).32 For the broad and featureless vasymCOO− band observed on TiO2_Merck no significant information was provided by such a method; in such a case the overall contribution of the formate species with respect to the HCOOH ones, responsible for the component at 1674 cm−1, was evaluated, gathering all possible vasymCOO− signals in one component (centered at 1598 cm−1). As a consequence, the possibility of establishing correlations between specific vasymCOO− and vsymCOO− components was prevented; yet, two limit pairing possibilities of the vasymCOO− components at lower frequencies can be considered, always taking into account the criterion based on the relative intensities of the vasymCOO− and vsymCOO− signals reported above:

i) the pairing with the vsymCOO− component at the lowest frequency, resulting in the maximum Δν with respect to vasymCOO−;

ii) the pairing with the vsymCOO− component at the highest frequency, resulting in the minimum Δν with respect to vasymCOO−.

On this account, the type i) pairings of the vasymCOO− components at 1541 and 1519 cm−1 obtained for TiO2_P25 with the vsymCOO− component at 1361 cm−1 provide a Δν splitting of 180 and 158 cm−1; these can be related to bridging/bidentate and bidentate formate species respectively, as HCOONa exhibits a Δν splitting of 201 cm−1.27

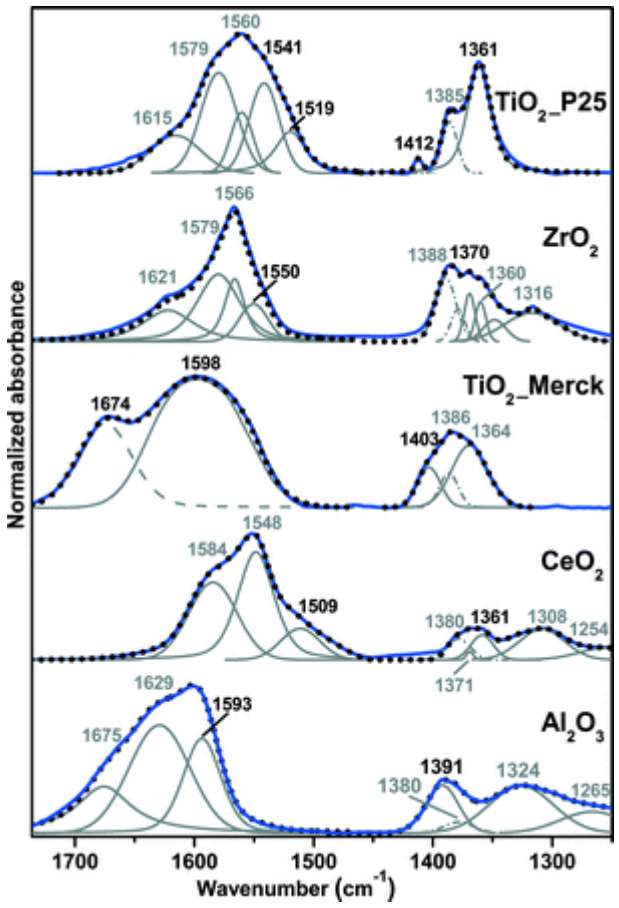


Fig. 5 IR spectra (Fig. 4; blue lines) and deconvolution analysis (grey lines) with the relative predicted spectra (dotted black lines).

In the case of ZrO2, the recognition of the components due to the bridging/bidentate formates might result only from type ii) pairings between the vasymCOO− component at 1550 cm−1 and the highest frequency vsymCOO− component at 1370 cm−1 (Δν, 180 cm−1).

The same occurs by considering components at 1548 and 1371–1361 cm−1 for CeO2 (Δν, 177–187 cm−1, bridging/bidentate); the presence of the bidentate formate might be indicated by the pairing between the vasymCOO− components at 1509 cm−1 with the vsymCOO− components at 1371–1361 cm−1 (Δν, 138–148 cm−1). In any case, the vasymCOO− components of the bridging/bidentate and bidentate formates on both ZrO2 and CeO2 constitute a small fraction of the overall vasymCOO− pattern in comparison with TiO2_P25. Finally, the narrowest Δν splitting of 202 cm−1 (1593–1391 cm−1) calculated for γ-Al2O3 indicates the presence of bridging formates whilst bidentate species can be excluded.27 Also the main vasymCOO− component at 1629 cm−1 can be attributed to bridging species if paired with the vsymCOO− component at 1391 cm−1 (Δν = 238 cm−1), or even to unidentate species (Scheme 2) if vsymCOO− at lower frequencies are considered. For TiO2_Merck the vsymCOO− at higher frequencies is centered at 1403 cm−1, while the broad vasymCOO− pattern extends down to 1515 cm−1, indicating that bidentate formates might be present. However, considering the maximum at 1598 cm−1, a Δν of 195 cm−1 suggests a prevalent presence of bridging formates. As for propanoic acid, the different amounts of the various types of formates on TiO2_P25 and TiO2_Merck are still related to their significantly different surface structures.26 Additional evidence on the different structures of formate on the two titania catalysts are obtained from the ratio between the sum of the integrated intensities of all the vsymCOO− components (Isym) and the analogous for vasymCOO− (Iasym). The values obtained were 0.3 and ca. 0.2 for TiO2_P25 and TiO2_Merck

respectively, representing the average Isym/Iasym values for the various types of formate present in the two cases. It is worthwhile to note that the database for such calculations (Table S3 in the ESI†) was obtained by minimizing the contribution of the δO–C–H mode in the deconvolution of the 1450–1300 cm−1 pattern in the case of TiO2_Merck and, vice versa, maximizing it in the case of TiO2_P25. The above values of the Isym/Iasym ratio can then be considered as the closest ones within the variability of the fitting procedure. The average angles between the C–O moieties of the formates on TiO2_P25 and TiO2_Merck are found to be ca. 120° and 130°, respectively.31 These values are consistent with those reported by Deacon and Phillips for a series of acetate complexes (Fig. S2 in the ESI†).28 In fact, only bridging species feature angles larger than 123°; then, also considering the differences between acetates and formates, it can be argued that bridging species might be prevalent on TiO2_Merck. Angle values in the range of 118–123° appeared common to bridging and bidentate acetates, while the latter selectively exhibit angles between 118 and 109°; thus, an average value of 120° for formates on TiO2_P25 accounts for a mixture of formate structures containing significant amounts of bidentate formates.

## 4 Conclusions

• The reactivity of various catalytic oxide materials (T, 383 K) in the direct synthesis of N-phenylpropionamide from propanoic acid and aniline has been assessed.

• Chemical and surface properties determine the amidation functionality of the studied systems:

TiO2_P25 > ZrO2 ≈ CeO2 ≈ TiO2_Merck > γ-Al2O3

• A 0th-order kinetic dependence is related to a Langmuir–Hinshelwood reaction path under kinetic control of the product-desorption step.

• The reactivity of the studied oxides matches their ability to stabilize bidentate carboxylate intermediates.

• Bidentate carboxylates are much more reactive towards the nucleophilic attack of amines than both bridging and unidentate species.

## Acknowledgements

The University of Torino and the Compagnia di San Paolo are acknowledged for funding (project no. ORTO11RRT5). Dr. Marco Pazzi is gratefully acknowledged for the HR-MS analysis.

## Notes and references

1. K. Ishihara, Tetrahedron, 2009, 65, 1085
2. V. R. Pattabiraman and J. W. Bode, Nature, 2011, 480, 471
3. C. Grosjean, J. Parker, C. Thirsk and A. R. Wright, Org. Process Res. Dev., 2012, 16, 781.
4. L. Perreux, A. Loupy and F. Volatron, Tetrahedron, 2002, 58, 2155
5. Khalafi-Nezhad, A. Parhami, M. N. Soltani Rad and A. Zarea, Tetrahedron Lett., 2005, 46, 6879 .
6. E. Gelens, L. Smects, L. A. J. Sliedregt, B. J. van Steen, C. G. Kruse, R. Leurs and R. V. A. Orru, Tetrahedron Lett., 2005, 46, 3751
7. K. Arnold, A. S. Batsanov, B. Davies and A. Whiting, Green Chem., 2008, 10, 124.
8. Kumar, H. K. Akula and M. K. Lakshman, Eur. J. Org. Chem., 2010, 2709
9. Gnanaprakasam and D. Milstein, J. Am. Chem. Soc., 2011, 133, 1682 .
10. K. V. N. S. Srinivas and B. Das, J. Org. Chem., 2003, 68, 1165 .
11. J. W. Comerford, J. H. Clark, D. J. Macquarrie and S. W. Breeden, Chem. Commun., 2009, 2562 .
12. P. S. Chaudhari, S. D. Salim, R. V. Sawant and K. G. Akamanchi, Green Chem., 2010, 12, 1707.
13. K. Komura, Y. Nakano and M. Koketsu, Green Chem., 2011, 13, 828.
14. C. L. Allen, A. R. Chhatwal and J. M. J. Williams, Chem. Commun., 2012, 48, 666.

15. M. Tamura, T. Tonomura, K. Shimizu and A. Satsuma, Green Chem., 2012, 14, 717 .
16. J. Soulè, H. Miyamura and S. Kobayashi, J. Am. Chem. Soc., 2011, 133, 18550 .
17. J. W. Comerford, T. J. Farmer, D. J. Macquarrie, S. W. Breeden and J. H. Clark, ARKIVOC, 2012,(vii), 282–293 .
18. C. Deiana, Y. Sakhno, M. Fabbiani, M. Pazzi, M. Vincenti and G. Martra, ChemCatChem, 2013, 5, 2832.
19. H. Zou, Y. S. Lin, N. Rane and T. He, Ind. Eng. Chem. Res., 2004, 43, 3019.
20. H. S. Fogler, Elements of Chemical Reaction Engineering, Pearson Education, Inc., 4th edn, 2006, p. 839.
21. G. Busca, Phys. Chem. Chem. Phys., 1999, 1, 723.
22. Chorkendorff and J. W. Niemantsverdriet, Concepts of Modern Catalysis and Kinetics, WILEY-VCH GmbH & Co. KGaA, Weinheim, 2005.
23. L.-F. Liao, C.-F. Lien, D.-L. Shieh, F.-C. Chen and J.-L. Lin, Phys. Chem. Chem. Phys., 2002, 4, 4584.
24. Parmaliana, F. Frusteri, F. Arena, A. Mezzapica and V. Sokolovskii, Catal. Today, 1998, 46, 117 .
25. Cannilla, G. Bonura, F. Arena, E. Rombi and F. Frusteri, Catal. Today, 2012, 195, 32.
26. G. Martra, Appl. Catal., A, 2000, 200, 275
27. Nakamoto, Infrared and Raman Spectra of Inorganic and Coordination Compounds, Wiley, New York, 4th edn, 1986, pp. 232–233 .
28. G. B. Deacon and R. J. Phillips, Coord. Chem. Rev., 1980, 33, 227.
29. N. B. Colthup, L. H. Daly and S. E. Wiberley, Introduction to Infrared and Raman Spectroscopy, Academic Press, New York, 2nd edn, 1975, pp. 321–225 .
30. X. G. Chen, R. Schweitzerstenner, S. A. Asher, N. G. Mirkin and S. Krimm, J. Phys. Chem., 1995, 99, 3074.
31. P. S. Braterman, Metal Carbonyl Spectra, Academic Press, London, 1975, p. 64.
32. Handbook of Vibrational Spectroscopy, ed. J. M. Chalmers and P. R. Griffiths, Wiley, 2001, vol. 3, p. 64